Chinese Journal of Aeronautics, 2013,26(2): 495–500

Chinese Society of Aeronautics and Astronautics
& Beihang University

Chinese Journal of Aeronautics

cja@buaa.edu.cn
www.sciencedirect.com

Auto-normalization algorithm for robotic precision drilling system in aircraft component assembly

Tian Wei *, Zhou Weixue, Zhou Wei, Liao Wenhe, Zeng Yuanfan

College of Mechanical and Electrical Engineering, Nanjing University of Aeronautics and Astronautics, Nanjing 210016, China

Received 6 December 2011; revised 21 January 2012; accepted 12 March 2012
Available online 7 March 2013

KEYWORDS

Aircraft assembly;
Auto-normalization;
Industrial robots;
Normal vector detection;
Robotic precision drilling

Abstract A novel approach is proposed to detect the normal vector to product surface in real time for the robotic precision drilling system in aircraft component assembly, and the auto-normalization algorithm is presented based on the detection system. Firstly, the deviation between the normal vector and the spindle axis is measured by the four laser displacement sensors installed at the head of the multi-function end effector. Then, the robot target attitude is inversely solved according to the auto-normalization algorithm. Finally, adjust the robot to the target attitude via pitch and yaw rotations about the tool center point and the spindle axis is corrected in line with the normal vector simultaneously. To test and verify the auto-normalization algorithm, an experimental platform is established in which the laser tracker is introduced for accurate measurement. The results show that the deviations between the corrected spindle axis and the normal vector are all reduced to less than 0.5°, with the mean value 0.32°. It is demonstrated the detection method and the auto-normalization algorithm are feasible and reliable.

1. Introduction

With the demand for higher productivity, more flexibility and lower cost in aircraft assembly, articulated arm robots are playing a predominant role in automating manufacturing process.[1] The off-the-shelf industry robots in the aerospace manufacturing industry help to create a stable, reliable and efficient environment, by mature solutions including arc welding, water jet cutting, inspection, de-burring, painting, sealing, drilling and riveting, composites fabrication, etc.[2] Automatic drilling and riveting system based on robot has become an extensive tendency in place of traditional hand operations in aircraft industry.[3,4]

Nowadays, aircraft component assembly is mainly accomplished by riveting, the quality of which immediately impacts the performance and security of aircraft.[5] Precision of the connecting hole dominates the riveting quality to a large extent, especially the coherence between the spindle axis and the normal vector to machining area on aircraft skin.[6] If the centerline of riveting hole is not exactly vertical to product surface, bending stress will emerge at the joint and decrease static and dynamic intensity, as well as assembling reliability.[7,8] It is required that the unidirectional clearance between product abutting surface and rivet head should be less than 0.05 mm for connecting hole.[9] Owing to the robot positioning error, manufacturing and installation error of fixture and product

* Corresponding author. Tel.: +86 25 84891836.
E-mail address: tw_nj@nuaa.edu.cn (W. Tian).

Peer review under responsibility of Editorial Committe of CJA.

Production and hosting by Elsevier

1000-9361 © 2013 Production and hosting by Elsevier Ltd. on behalf of CSAA & BUAA. Open access under CC BY-NC-ND license.
http://dx.doi.org/10.1016/j.cja.2013.02.029

and random dynamic variation of product attitude in the workshop, there must be angle deviation between the normal vector and the tool axis. Consequently, it is essential to align the posture of product or spindle axis before drilling to assure drilling vertical precision.

Qin et al.[10] presented a three-point regulation algorithm specifically for NC drill and rivet equipment based on NC bracket, but it is not suitable for large size components with complex structure. Iovenitti et al.[11] developed a vector setting device for drill bushes to determine adjustment parameters required to align the arbitrary vector. Shan et al.[12] designed a 5-DOF spindle posture alignment mechanism and a method for prompt posture alignment of spindle was proposed for large suspended panel. These achievements contributed to drilling accuracy and efficiency, but the additional cost for regulating devices was raised simultaneously.

Robotic precise drilling technology has been applied by leading aircraft manufacturers in the world such as Boeing.[13] Further, Electroimpact Inc. has achieved a normality tolerance of $\pm 0.5°$.[14] However, interiorly the relative research is still on the primary stage. The focus of this paper is to study a novel method of detecting the actual normal vector and auto-normalizing by correcting the spindle axis direction for robotic precision drilling system. Its advantages are as follows:

(1) Spindle axis is adjusted only in direction by rotating on drilling position which is exactly set as the virtual tool center point (VTCP) of robot system, ensuring that drilling position remains stationary during adjustment process.
(2) Laser sensors applied in the system are installed not parallel to the spindle axis, and the inclined angle contributes to higher detecting precision and system structure simplification.

2. System description

2.1. The system

The robotic drilling precision system (RDPS) as shown in Fig. 1 mainly consists of robot, multi-function end effector, rail, fixture, etc. The 6-axis articulated robot can move along the 7th axis linear rail which is mounted to the floor to expand working space of the robot. The independently developed multi-function end effector (MFEE) is attached to the robot's wrist to perform a series of process such as scanning process datum, measuring normal vector, pressure foot clamping and loosening, drilling, reaming, countersinking, trimming, etc. It has been proved that the hanging configuration between the MFEE and the robot is more appropriate for drilling process in aircraft component assembly.[15] Moreover, varieties of special sensors are integrated into the MFEE for acquiring requisite data in real time during the drilling process, such as normality sensors, countersinking depth sensor, scanning sensor, etc.

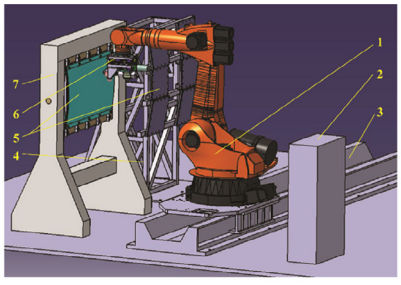

1—Robot; 2—Robot control cabinet; 3—Rail; 4—Rigid fix; 5—Test-piece; 6—End effector; 7—Flexible fixture

Fig. 1 Robotic drilling precision system.

Product to be drilled is held by the fixture to guarantee enough stiffness when bearing pressing force from the MFEE. Besides a control software tailored for the system is developed to manipulate and coordinate motions of the robot and the MFEE, acting as communication interface between the robot controller, the MFEE and the operator.

2.2. The process flow

In the RDPS, the robot and the MFEE chiefly undertake precision drilling process. The essential workflow, as shown in Fig. 2, is formulated on the basis of the process features of aircraft component assembly.

(1) Generate NC off-line program and import it into the system control software.
(2) Scan the product process datum (such as holes and bolts) to recognize the actual position of product by scanning sensors installed on the MFEE.
(3) Set up relationship between the robot base coordinate system and the real product coordinate system.
(4) Modify NC codes based on (2) and (3) to compensate the differences between the actual product and the product model in off-line programming system.
(5) Move the robot to the *i*th hole position to drill on the product surface based on the updated program.
(6) Detect the normal vector by normality sensors; send commands to the robot to normalize the MFEE.
(7) The MFEE performs a series process of clamping, drilling, reaming, countersinking, cooling, etc.

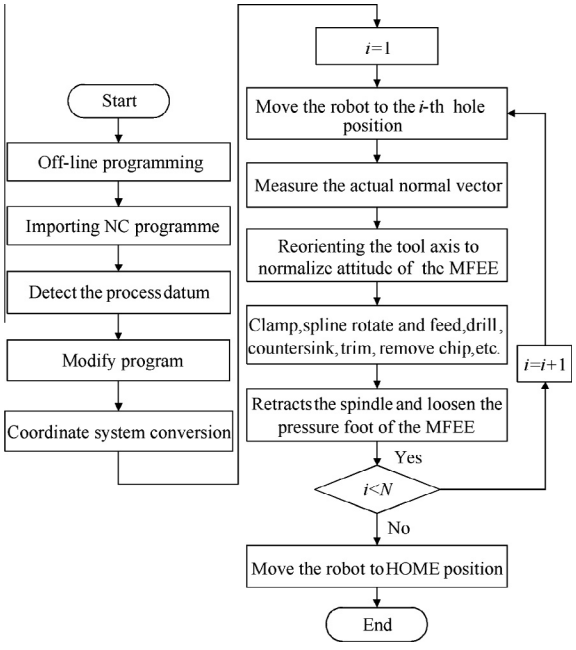

Fig. 2 Workflow of robotic drilling process.

(8) Retract the spindle and loosen the pressure foot after the ith hole is bored out.
(9) An integrated drilling cycle from (5) to (8) is completed, move the robot to HOME position which is far away from the product after all holes are drilled.

3. Implementation of auto-normalization

A basic hypothesis has been introduced into the auto-normalization method in order to reduce the computational complexity, i.e. that aircraft skin with curved surface is considered to be made up by numerous tiny planes and the small area near the drilling position is a flat plane. On the strength of the hypothesis, a scheme to detect the actual normal vector to product surface is designed. As shown in Fig. 3, the detection system at the head of the MFEE is composed of four non-contact laser displacement sensors installed in cruciform structure. Furthermore, the four laser beams distribute on a virtual conic surface, the cone angle of which can be symbolized as λ and the central axis of which is exactly the spindle axis. In consequence, the four beams can draw close enough without crossing to ensure that the envelope size of the four projection points on the product surface can be small enough for required measurement accuracy.

At the beginning of the robotic drilling process, the robot moves to planned point location according to the NC program written by off-line programming system. The cutter built into the MFEE gets close to the product in theoretical normal direction. Then the distances to the skin surface are measured by the four laser sensors. With that, the deviation between the normal vector and the spindle axis is computed. If the deviation exceeds a specified threshold, then calculate the robot target attitude via the auto-normalization algorithm. Then, reorient the robot attitude through pitch and yaw rotations on the VTCP to correct the direction of the spindle axis.

The auto-normalization method for RDPS in aircraft component assembly is briefly explained as follows:

Step 1: Capture the distance data from the four laser displacement sensors.

Step 2: Calculate the deviation between the spindle axis and the normal vector to product surface.

Step 3: Evaluate and output the robot target posture when the deviation is overlarge.

Step 4: Adjust the robot to the target attitude to correct the spindle axis precisely enough.

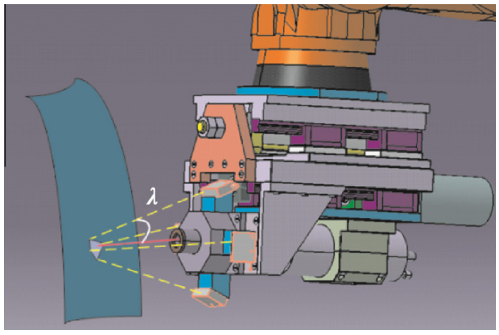

Fig. 3 Normal vector detection system.

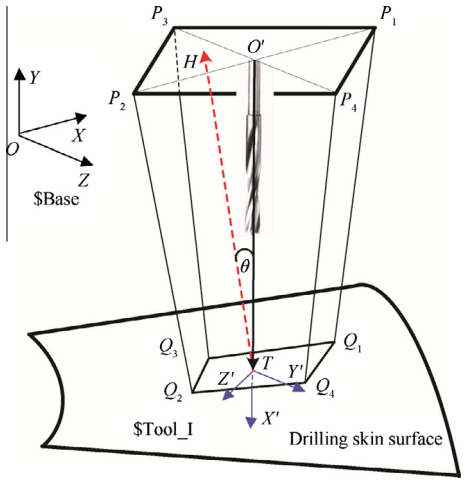

Fig. 4 Geometric model.

4. Algorithm of auto-normalization

4.1. Geometric model of detecting normal vector

As shown in Fig. 4, the geometric model is extracted from the physical model of the normal vector detection system. For expressing conveniently, the robot base coordinate system is named as \$Base; the unadjusted tool coordinate system, \$Tool_I. Assume that the robot original attitude is (a, b, c) and the target attitude needed to solve is (a', b', c').

In Fig. 4, the point T represents the VTCP, i.e. the origin of \$Tool_I; the vector $\overrightarrow{O'T}$ signifies the spindle axis approaching direction, i.e. $+X'$-axis of \$Tool_I. P_1, P_2, P_3 and P_4 are the measure starting points of the four sensors; the projective points on the product surface are Q_1, Q_2, Q_3 and Q_4, respectively. The distances acquired from the sensors are set as $\overline{P_1Q_1} = h_1$, $\overline{P_2Q_2} = h_2$, $\overline{P_3Q_3} = h_3$ and $\overline{P_4Q_4} = h_4$. The two opposite laser beams (such as $\overrightarrow{P_1Q_1}$ and $\overrightarrow{P_2Q_2}$ $\overrightarrow{P_3Q_3}$ and $\overrightarrow{P_4Q_4}$) are coplanar with $\overrightarrow{O'T}$; the plane $\overline{P_1Q_1P_2Q_2}$ is needed to be perpendicular to the plane $\overline{P_3Q_3P_4Q_4}$. In addition, $+Z'$ -axis of \$Tool_I is defined in the plane $\overline{P_1Q_1P_2Q_2}$; $+Y'$ -axis of \$Tool_I, $\overline{P_3Q_3P_4Q_4}$. Supposing the outer normal vector to the drilling skin surface is shown as $\overrightarrow{TH}$, the angle θ stands for the intersection angle between $\overrightarrow{O'T}$ and $\overrightarrow{TH}$.

4.2. Deviation calculation

Since the angle θ is defined as the intersection angle between the spindle axis and the normal vector to the drilling skin surface, the problem to normalize the spindle axis direction can be simplified as minimizing the angle θ. The space geometry relationship between θ and θ_1, θ_2 is shown in Fig. 5. $\overrightarrow{TM}$ is the projection of $\overrightarrow{TH}$ on the $X'TY'$ coordinate plane; $\overrightarrow{TN}$ is the projection of $\overrightarrow{TH}$ on the $X'TZ'$ coordinate plane, where the point M and N are separately on the line of $\overline{P_3P_4}$ and $\overline{P_1P_2}$. Let θ_1 be the angle from $\overrightarrow{TO'}$ to $\overrightarrow{TN}$, θ_2 be the angle from $\overrightarrow{TO'}$ to $\overrightarrow{TM}$, and t_1 be the angle from $\overrightarrow{TM}$ to $\overrightarrow{TH}$. The angle θ is a constantly positive scalar; the angle θ_1, θ_2 and t_1 have both positive and negative sides, which are defined as follows: the rotation around $+Y'$ -axis is the positive direction of θ_1 and t_1; the rotation around $+Z'$ -axis is the positive direction of θ_2.

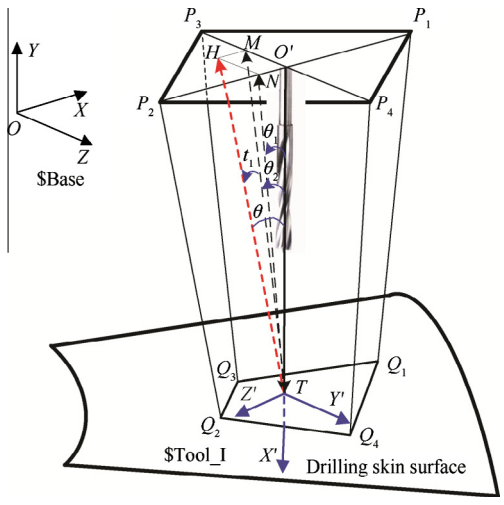

Fig. 5 Space geometry relationship between θ and θ_1, θ_2.

(1) Relationship between θ and θ_1, θ_2

Assume that the coordinates of point H is (x_0, y_0, z_0) in \$Tool_I .The relationship between θ and θ_1, θ_2 is presented as follows:

$$\tan\theta = \frac{\sqrt{z_0^2 + y_0^2}}{|O'T|} \tag{1}$$

$$\tan\theta_1 = \frac{z_0}{|O'T|} \tag{2}$$

$$\tan\theta_2 = \frac{-y_0}{|O'T|} \tag{3}$$

According to the three equations above, we can obtain

$$\theta = \arctan\sqrt{\tan^2\theta_1 + \tan^2\theta_2} \tag{4}$$

$$t_1 = \arctan(\cos\theta_2 \times \tan\theta_1) \tag{5}$$

(2) Relationship between θ_1, θ_2 and h_1, h_2, h_3, h_4

The projection relationship of the angle θ_1 on the $X'TZ'$ coordinate plane of \$Tool_I is shown in Fig. 6. The distance between P_1 and P_2 is symbolized by l_{12}; the distance between P_3 and P_4, l_{34}.

We can get

$$\overline{AQ_1} = h_1 \times \cos\lambda \tag{6}$$

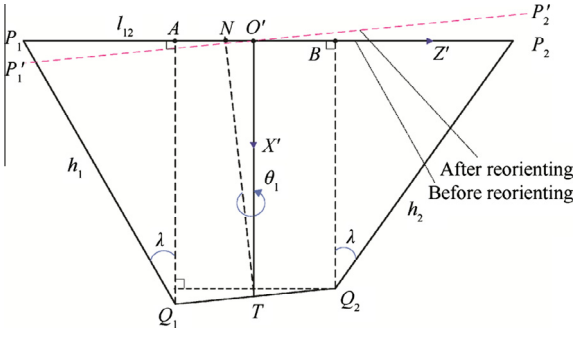

Fig. 6 Relationship between θ_1 and h_1, h_2.

$$\overline{BQ_2} = h_2 \times \cos\lambda \tag{7}$$

$$\overline{AB} = l_{12} - h_1 \times \sin\lambda - h_2 \times \sin\lambda \tag{8}$$

$$\tan\theta_1 = \frac{\overline{BQ_2} - \overline{AQ_1}}{\overline{AB}} = \frac{(h_2 - h_1) \times \cos\lambda}{l_{12} - (h_1 + h_2) \times \sin\lambda} \tag{9}$$

Thus,

$$\theta_1 = \arctan\frac{(h_2 - h_1) \times \cos\lambda}{l_{12} - (h_1 + h_2) \times \sin\lambda} \tag{10}$$

By the same logic,

$$\theta_2 = \arctan\frac{(h_3 - h_4) \times \cos\lambda}{l_{34} - (h_3 + h_4) \times \sin\lambda} \tag{11}$$

Substituting Eqs. (10), (11) into Eq. (4), we can learn

$$\theta = \arctan\sqrt{\frac{(h_1 - h_2)^2 \times \cos^2\lambda}{[l_{12} - (h_1 + h_2) \times \sin\lambda]^2} + \frac{(h_3 - h_4)^2 \times \cos^2\lambda}{[l_{34} - (h_3 + h_4) \times \sin\lambda]^2}} \tag{12}$$

4.3. Inverse solution of target attitude

The adjusted tool coordinate system is named as \$Tool_II. Comparison of \$Tool_I and \$Tool_II is illustrated in Fig. 7. It is known that the spindle axis $\overrightarrow{O'T}$ can be coincident with the outer normal vector $\overrightarrow{TH}$ via twice Cartesian coordinate rotation transformation about the VTCP, i.e. pitch and yaw rotations. The transformation from \$Tool_I to \$Tool_II can be described by the matrix of ${}^{\$Tool\_I}_{\$Tool\_II}\boldsymbol{R}$, i.e.,

$$\begin{aligned}
{}^{\$Tool_I}_{\$Tool_II}\boldsymbol{R} &= \mathrm{Euler}(\theta_2, t_1, 0) \\
&= \mathrm{Rot}(z, \theta_2) \cdot \mathrm{Rot}(y, t_1) \cdot \mathrm{Rot}(x, 0) \\
&= \begin{bmatrix} \cos\theta_2 & -\sin\theta_2 & 0 \\ \sin\theta_2 & \cos\theta_2 & 0 \\ 0 & 0 & 1 \end{bmatrix} \\
&\quad \cdot \begin{bmatrix} \cos t_1 & 0 & \sin t_1 \\ 0 & 1 & 0 \\ -\sin t_1 & 0 & \cos t_1 \end{bmatrix} \cdot \begin{bmatrix} 1 & 0 & 0 \\ 0 & 1 & 0 \\ 0 & 0 & 1 \end{bmatrix}
\end{aligned} \tag{13}$$

The robot target attitude in \$Base can be inversely solved by means of the transformation relationships between \$Base, \$Tool_I and \$Tool_II, i.e.,

$${}^{\$Base}_{\$Tool\_II}\boldsymbol{R} = {}^{\$Base}_{\$Tool\_I}\boldsymbol{R} \cdot {}^{\$Tool\_I}_{\$Tool\_II}\boldsymbol{R} \tag{14}$$

$$\begin{aligned}
\mathrm{Euler}(a', b', c') &= \mathrm{Euler}(a, b, c) \cdot \mathrm{Euler}(\theta_2, t_1, 0) \\
&= \begin{bmatrix} \cos a & -\sin a & 0 \\ \sin a & \cos a & 0 \\ 0 & 0 & 1 \end{bmatrix} \cdot \begin{bmatrix} \cos b & 0 & \sin b \\ 0 & 1 & 0 \\ -\sin b & 0 & \cos b \end{bmatrix} \\
&\quad \cdot \begin{bmatrix} 1 & 0 & 0 \\ 0 & \cos c & -\sin c \\ 0 & \sin c & \cos c \end{bmatrix} \cdot \begin{bmatrix} \cos\theta_2 & -\sin\theta_2 & 0 \\ \sin\theta_2 & \cos\theta_2 & 0 \\ 0 & 0 & 1 \end{bmatrix} \\
&\quad \cdot \begin{bmatrix} \cos t_1 & 0 & \sin t_1 \\ 0 & 1 & 0 \\ -\sin t_1 & 0 & \cos t_1 \end{bmatrix} \cdot \begin{bmatrix} 1 & 0 & 0 \\ 0 & 1 & 0 \\ 0 & 0 & 1 \end{bmatrix} \\
&= \begin{bmatrix} n_x & o_x & a_x \\ n_y & o_y & a_y \\ n_z & o_z & a_z \end{bmatrix}
\end{aligned} \tag{15}$$

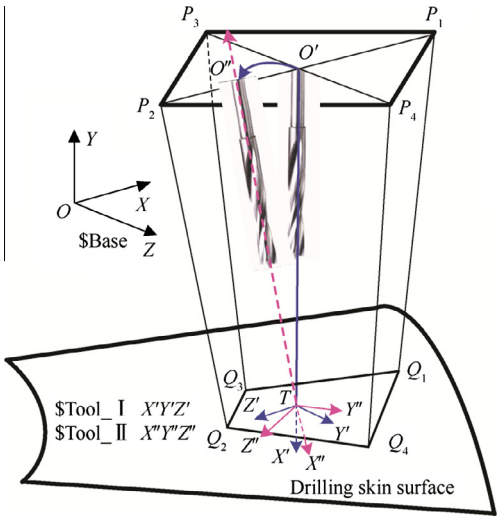

Fig. 7 Comparison of unadjusted and adjusted tool coordinate systems.

In formula (15), n_x, n_y, n_z are the coordinates in \$Base of unit vector in $+X''$ direction of \$Tool_II; o_x, o_y, o_z are the coordinates in \$Base of unit vector in $+Y''$ direction of \$Tool_II; a_x, a_y, a_z are the coordinates in \$Base of unit vector in $+Z''$ direction of \$Tool_II.

It is necessary to note that there is always more than one sequence of rotations about the three principle axes that results in the same orientation of an object; all possible solutions of Euler angles (a', b', c') from a rotation matrix can be obtained as follows:

$n_z \neq \pm 1$ Case: There are actually two sets of distinct solutions in the non-degenerate case of $b' \neq \pm \pi/2$.

$$\begin{cases} b' = \mathrm{a\,tan\,2}(-n_z, \sqrt{n_x^2 + n_y^2}), \text{where } \cos b' > 0 \\ a' = \mathrm{atan2}(n_y/\cos b', n_x/\cos b') \\ c' = \mathrm{a\,tan\,2}(o_z/\cos b', a_z/\cos b') \end{cases} \tag{16}$$

or

$$\begin{cases} b' = \mathrm{a\,tan\,2}(-n_z, -\sqrt{n_x^2 + n_y^2}), \text{where } \cos b' < 0 \\ a' = \mathrm{a\,tan\,2}(n_y/\cos b', n_x/\cos b') \\ c' = \mathrm{a\,tan\,2}(o_z/\cos b', a_z/\cos b') \end{cases} \tag{17}$$

For the degenerate case of $b' = \pm\pi/2$, an infinite number of solutions exist; the link relationship between a' and c' is described in the following formulas.

$n_z = -1$ Case :

$$\begin{cases} b' = \pi/2 \\ c' = a' + \mathrm{a\,tan\,2}(o_x, a_x) \end{cases} \tag{18}$$

$n_z = 1$ Case :

$$\begin{cases} b' = -\pi/2 \\ c' = -a' + \mathrm{a\,tan\,2}(-o_x, -a_x) \end{cases} \tag{19}$$

In practice, one definite solution is often needed. For this task, it is convenient to set $a' = 0$ and compute c' as described above.

Eventually, the target attitude angles (a', b', c') are imported to the system control software to implement the auto-normalizing process by reorienting the spindle axis.

4.4. Calibration method of detection system

There inevitably exist differences between the physical model of the detection system and the theoretical one. These differences are chiefly caused by manufacturing errors of the four sensors and their mounting brackets, as well as assembly errors. The composite error with high spatial complexity is not available by means of general measurement methods. Therefore a FARO laser tracker is introduced to measure and calibrate the various styles of errors. The main procedures are as follows:

Step 1: Adjust and clamp each laser sensor according to current tool coordinate system measured by the laser tracker.

Step 2: Measure every subentry error on coordinate planes to obtain the actual parameters required in the formulas presented in the preceding text.

Step 3: Modify these formulas reasonably and verify the precision of the detecting system with updated formulas.

5. Experiment and verification

To test and verify the auto-normalization algorithm above, an experimental platform was built up, as shown in Fig. 8. The experimental platform mainly consists of the RDPS, three test pieces and the measuring equipment, i.e. a 3-DOF FARO laser tracker utilized for high accurate measurement.

Firstly, calibrate the normal vector detecting system to compensate installation errors of the normality sensors. Secondly, measure the actual normal direction to the drilling area on the test pieces by the laser tracker. Then, move the robot in arbitrary attitude to the test pieces and measure the deviation between the normal vector and the spindle axis before adjusting. Simultaneously, record the distance values of the four laser displacement sensors and calculate the robot target attitude by the auto-normalization algorithms method. Finally, adjust the robot to the calculated attitude and measure the deviation between the normal vector and the reoriented spindle axis by the laser tracker.

Three trials were conducted on each piece and the experimental results are shown in Table 1.By analyzing and comparing the experimental results above, it can be seen that the deviations between the normal vector and the reoriented

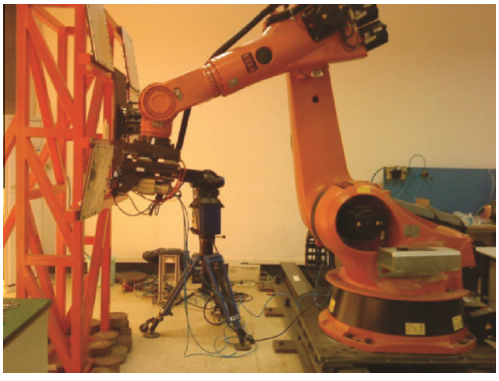

Fig. 8 Experimental platform.

Table 1 Experimental results.

Test piece	Before orientation (deg)			After orientation (deg)		
	Attitude		Deviation	Attitude		Deviation
	a	*b*		*a*	*b*	
Test piece 1	−3.37	−7.68	3.89	−1.21	−10.6	0.33
	0.93	−14.98	4.64	−1.17	−10.7	0.28
	−3.99	−6.43	5.19	−1.31	−10.9	0.45
Test piece 2	4.80	−3.58	5.69	0.062	0.01	0.16
	−2.4	4.22	5.08	−0.02	−0.00	0.23
	−4.6	4.88	6.99	0.299	−0.29	0.29
Test piece 3	−3.34	5.32	4.40	−1.35	9.88	0.35
	3.16	4.82	6.36	−1.02	9.32	0.47
	3.42	11.81	4.70	−0.77	9.54	0.30

spindle axis are all reduced to less than 0.5°, with the mean value 0.32°, which is able to meet technical requirements for practical application in aircraft industry.

6. Conclusions

(1) A method to detect the normal vector to product surface in real time is proposed and the corresponding detection system is developed in the paper. The deviation between the normal vector to the drilling skin surface and the spindle axis is measured by four laser displacement sensors.
(2) An auto-normalization algorithm is presented to correct the attitude of the MFEE which is fixed to the robot's wrist, meanwhile leaving the drilling hole position stationary. The adjusting process of the robot attitude is performed via pitch and yaw rotations by definite angle on the VTCP.
(3) An experimental platform is built up and a series of experiments are conducted. The experimental results indicate that the angle deviation between product normal vector and adjusted spindle axis is limited within 0.5°, with the mean value 0.32°.
(4) The reorienting accuracy is directly bound up with the precision of normality sensors; consequently, high-precision displacement sensors contribute to enhancing the normalizing accuracy.

Acknowledgments

The authors are grateful to the technicians in Chengdu Aircraft Industrial Group Corporation in AVIC. They would also like to thank the anonymous reviewers for their critical and constructive review of the manuscript. This study was co-supported by Key Technology Research and Development Program of Jiangsu Province, China (No. BE2011178) and the Aviation Industry Innovation Fund (No. AC2011214).

References

1. Summers M. Robot capability test and development of industrial robot positioning system for the aerospace industrial. *SAE Trans* 2005;**114**(1):1108–18.
2. Devlieg R, Szallay T. Applied accurate robotic drilling for aircraft fuselage. *SAE Int J Aerosp* 2010;**3**(1):180–6.
3. Bi SS, Liang J. Robotic drilling system for titanium structures. *Int J Adv Manuf Technol* 2011;**54**:767–74.
4. Olsson T, Robertsson A, Johansson R. Flexible force control for accurate low-cost robot drilling. In: *2007 IEEE international conference on robotics and automation*. 2007. p. 4770–5.
5. Qu WW, Dong HY, Ke YL. Pose accuracy compensation technology in robot-aided aircraft assembly drilling process. *Acta Aeronautica et Astronautica Sinica* 2011;**32**(10):1951–60 [Chinese].
6. Du ZC. Measurement method for evaluating normal direction of surface for digital drilling and riveting. *Aeronautical Manuf Technol* 2011;**22**:108–11 [Chinese].
7. Xue HJ, Zhang JP. Normal measurement and adjustment for skin drilling. *J Aeronautical Manuf Technol* 2011;**23**:60–2, 66 [Chinese].
8. Ying GM, Wang ZQ, Kang YG. Study on normal vector measurement method in auto-drilling & riveting of aircraft panel. *Mach Tool Hydraulics* 2010;**38**(23):1–4, 8 [Chinese].
9. Chief Edition Committee of Handbook of Aerospace Manufacture Engineering. *Handbook of Aerospace Manufacture Engineering: Aircraft Assembly*. Beijing: Aviation Industry Press; 1993 [Chinese].
10. Qin XS, Wang WD, Lou AL, Wei T. Three-point bracket regulation algorithm for drilling and riveting of aerofoil. *Acta Aeronautica et Astronautica Sinica* 2007;**28**(6):1455–60 [Chinese].
11. Iovenitti PG, Mutapcic E, Nagarajah CR. Positioning and orienting a drill axis on a curved surface. *J Adv Manuf Technol* 2001;**17**:484–8.
12. Shan YC, He N, Li L, Yang YF. Realization of spindle prompt normal posture alignment for assembly hole-making on large suspended panel. In: *2001 third international conference on measuring technology and mechatronics automation*. 2011. p. 956–60.
13. Devlieg R, Feikert E. One-up assembly with robots. In: *SAE 2008 aerospace manufacturing and automated fastening conference*. 2008. p. 2297.
14. Devlieg R. Robotic trailing edge flap drilling system. *Aerosp Technol Conf Exposition* 2009. p. 3324.
15. Liang J, Bi SS. Effects of drill end effector's mounted method on the robot performance. *J Mech Eng* 2010;**46**(21):13–8 [Chinese].

Tian Wei received B.S., M.S. and Ph.D. degrees from Nanjing University of Science and Technology Institute in 2000, 2003 and 2006 respectively, and then became a teacher in Nanjing University of Aeronautics and Astronautics. Now he is an associate professor. His main research interests are digital flexible assembly, green remanufacturing, and so on.